Comprehensive Kinetics Investigation of Methane Adsorption in MOF-5: Insights from Molecular Dynamics

Haonan Chen
Department of Advanced Environmental Science and Engineering, Faculty of Engineering Sciences, Kyushu University

Miyazaki, Takahiko
Department of Advanced Environmental Science and Engineering, Faculty of Engineering Sciences, Kyushu University

Kyaw Thu
Department of Advanced Environmental Science and Engineering, Faculty of Engineering Sciences, Kyushu University

https://doi.org/10.5109/7342440

出版情報：Evergreen. 12 (1), pp.81-89, 2025-03. 九州大学グリーンテクノロジー研究教育センター
バージョン：

Comprehensive Kinetics Investigation of Methane Adsorption in MOF-5: Insights from Molecular Dynamics

Haonan Chen[1,*], Takahiko Miyazaki[1,2], Kyaw Thu[1,2,*]

[1]Department of Advanced Environmental Science and Engineering, Faculty of Engineering Sciences, Kyushu University, Kasuga-koen 6-1, Kasuga, 816-8580, Fukuoka, Japan

[2]Research Center for Next Generation Refrigerant Properties (NEXT-RP), International Institute of Carbon-Neutral Energy Research (WPI-I2CNER), Kyushu University, 744 Motooka, Nishi-ku, Fukuoka, 819-0395, Fukuoka, Japan

*Author to whom correspondence should be addressed:
E-mail: chen.haonan.732@s.kyushu-u.ac.jp, kyaw.thu.813@m.kyushu-u.ac.jp

(Received December 13, 2024; Revised January 13, 2025; Accepted January 16, 2025).

Abstract: With the advancement of porous materials, physical adsorption has found extensive applications in environmental and energy-related fields. However, capturing the detailed adsorption process through experiments remains challenging, and comprehensive studies of adsorption kinetics using molecular simulations are still limited. This study employs molecular dynamics simulations to investigate methane adsorption in MOF-5 across temperatures (200 K, 270 K, 300 K) and pressures (5–50 bar). Equilibrium adsorption uptake agrees well with experimental data, where the mean relative error is less than 6 %, validating the simulation approach. Adsorption energy and self-diffusion coefficients reveal the saturation of high-energy sites at low pressure and the transition of methane to a supercritical state with reduced mobility at higher densities. Adsorption dynamics curves, fitted with Sultan's model, generally match the simulations but give higher initial value in high-pressure stages, reflecting model limitations, where the root mean square is around 0.1-0.3. Correlation analysis highlights the relationships among fitting parameters and equilibrium adsorption properties. Radial distribution functions reveal structural transitions, including multilayer adsorption and phase tendencies influenced by temperature and pressure. This comprehensive study demonstrates the effectiveness of molecular dynamics in modeling adsorption processes, offering insights into equilibrium properties, kinetics, and phase behavior, and providing a robust framework for future adsorption research.

Keywords: Adsorption kinetics; Methane; MOF; Molecular dynamics; Diffusion; Adsorption energy; Porous material

1. Introduction

Physical adsorption is a spontaneous process in which gas or liquid molecules are adsorbed on the surface of the adsorbent due to the van der Waals and electronic interactions. With the development of porous material, it has broad applications[1-3]. Activated carbon, due to its low cost, high efficiency, and regeneration, is widely applied in the purification, including carbon capture and utilization field[4-6]. The raw materials of activated carbon include biomass, coal, industrial waste, etc., which are very easy to obtain[7]. Activated carbon is highly disordered, so customization is hard. However, molecular sieve, a zeolite-based material with selectivity for adsorbate, has been utilized in gas separation[8-10]. Meanwhile, with the good heat stability of the molecular sieve, it can be used in thermal energy utilization, such as adsorption heat transformer or adsorption heat pump systems[11-13]. 2-D materials, graphene and nanotubes, with a functionalizable surface, are effective in pollutant treatment for liquid[14-16]. After that, metal-organic frameworks (MOFs) are a class of porous polymers constructed by combining organic ligands with inorganic metal ions to form three-dimensional structures and can be fully customized[17-19]. With the standardized synthesis process and highly consistent structure, MOFs are expected to be applied in industrial gas storage systems[20-22].

The experimental investigations for adsorption focus on the adsorption capacities and many analytical models are developed to evaluate the adsorption isotherm[23-25]. Besides, researchers use adsorption kinetics to illustrate the adsorbate diffusion for the adsorption mechanism. Some models are concluded as well: The linear driving force model (LDF), which contains the mass transfer coefficient, is the earliest kinetic model with widespread

feasibility[26]. The LDF model is also close to the pseudo-first-order model (PFO), and there is a pseudo-second-order model (PSO) that can describe the adsorption kinetics, especially for chemical or slow adsorption[27]. The Fickian diffusion model (FD), which uses the concentration gradient, but the temperature gradient is neglectable, has been applied in a fast adsorption process[28]. The semi-infinite model describes the adsorption in the initial period with high accuracy[29].

However, most experimental research cannot give microscopic insight into the adsorption process. There are several computational methods to simulate the adsorption process at molecular level, including the Grand Canonical Monte Carlo (GCMC) and molecular dynamics (MD). GCMC can obtain the saturated conditions of adsorption. Ke et al. utilized GCMC simulations and the Ideal Adsorbed Solution Theory to investigate the adsorption uptake of ethane and ethene in ZIF-8, ZIF-8_R3m, and ZIF-8_Cm, revealing the impact of polymorphic isomers on the competitive adsorption of these molecules[30]. Li et al. employed machine learning-assisted high-throughput screening to compute the separation performance of MOFs for CH_4/C_2H_6 and CH_4/CO_2 mixtures in bulk, which quantified the impact of metal center sites on separation performance[31]. Saren et al. applied GCMC in the carbon dioxide adsorption in graphitic slit-pores with different functional groups, and gave a detailed discussion of the adsorbed carbon dioxide orientations[32].

MD is able to explore detailed particle behavior and transient properties. Swaipram et al. used MD simulations to investigate methanol's distribution and diffusion behavior within the flexible MIL-88B-Cl framework. They observed that, with increasing loading, methanol transitions from being preferentially distributed around counterions with higher mobility to aggregating near the hydrophobic linker regions of the MOF, where it forms stable hydrogen bonds. However, the increase in loading does not affect the isotropic nature of its diffusion[33]. Chen et al. investigated the thermal conductivity changes for both adsorbate and adsorbent. They found that in the adsorption process, the movement of adsorbate was constrained by the adsorbent and decreased the thermal conductivity. While the atomic oscillation of adsorbent was enhanced by adsorbate, leading to an increase in the thermal conductivity[34].

Current research on the kinetics of physical adsorption using molecular simulations remains relatively limited, which focus on the adsorption kinetics itself without considering relative physical properties. In this study, we employed molecular dynamics simulations to investigate the adsorption of methane in MOF-5. MOF-5 is a representative MOF with simple structure and plenty of experimental studies to validate the simulation results. First, the equilibrium adsorption uptake from the simulations was validated against experimental data. We then analyzed the effects of temperature and pressure by examining the adsorption energy and self-diffusion coefficients of adsorbed methane. Subsequently, the adsorption kinetics were fitted to evaluate the correlations among the parameters of the fitting equation. Finally, the phase state of the adsorbed phase was explored using radial distribution functions (RDFs). This study provides a more comprehensive demonstration of the application of molecular dynamics in the study of physical adsorption.

2. Computational Methodology

2.1 Molecular structure

Methane is a nonpolar molecule with a symmetrical tetrahedral structure, so its charge distribution is uniform. Since there is no obvious dipole moment, the electrostatic force within the molecule is very small. Therefore, the lack of polar interactions provides theoretical support for simplifying the model of methane as a coarse-grained single atom.

MOF-5 framework, synthesized with zinc ion and terephthalic acid, contains large porous with radius of 8 Å. In molecular configuration, it has a porosity of 0.8037 and density of 593.40 kg/m^3, extending from a 2-2-2 unit cell, where the cubic length is measured in 51.6640 Å[35].

2.2 Molecular interactions

The interaction between the methane and MOF-5 is described by Lennard-Jones (LJ) potential, which is widely applied to express van der Waal's force in the adsorption field, as shown in Equation (1),

$$u(r_{ij}) = \begin{cases} 4\varepsilon\left[\left(\frac{\sigma}{r_{ij}}\right)^{12} - \left(\frac{\sigma}{r_{ij}}\right)^{6}\right] & r_{ij} < r_c \\ 0 & r_{ij} \geq r_c \end{cases} \quad (1)$$

where i, j, denote two different atoms respectively, u is the intermolecular potential, ε is energy well depth and σ is van der Waals radius, r is the distance of separation between two atoms. r_c is the cutoff, beyond which the interaction is neglected. Lorentz-Berthelot mixing rules are utilized to obtain the parameters with different kind of molecules according to Equations (2) and (3)[36],

$$\varepsilon_{ij} = \sqrt{\varepsilon_i \varepsilon_j} \quad (2)$$

$$\sigma_{ij} = \frac{\sigma_i + \sigma_j}{2} \quad (3)$$

The LJ parameters are referred from the universal force field (UFF), and DREIDING[37,38].

2.3 Simulation details

All the MD simulations are conducted by the Large-scale Atomic/Molecular Massively Parallel Simulator (LAMMPS)[39]. Each simulation is operated in periodic boundary conditions, with a cutoff of 12 Å, Canonical (NVT) ensemble regulated by Nosé-Hoover thermostat, and the timestep is 1 fs[40]. The bulk conditions include three temperatures: 200 K, 270 K, and 300 K, where the

pressure ranges from 5 bar to 50 bar. The simulation consists of two stages: adsorption simulation and equilibrium simulation.

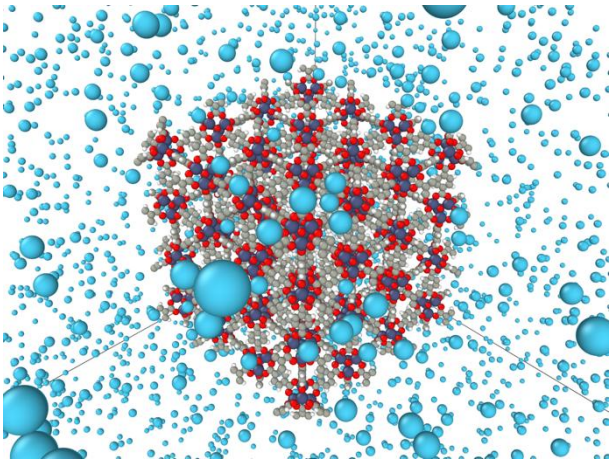

Fig. 1: The schematic of adsorption simulation.

In adsorption simulations, the adsorbate ambient is prepared first. According to the density of a given condition, a certain number of methane molecules are created in a cubit box with a length of 400 Å, to ensure the proceeding adsorption makes a neglectable effect on the bulk pressure. All adsorbate ambient is in the gaseous phase based on NIST/REFPROP[41]. The gas simulations proceed with 1 ns relaxation and 2 ns production. Then, a MOF-5 framework is inserted into the center of the methane ambient and frozen. The methane molecules in the region of the framework are deleted to guarantee the initial uptake is zero. After that, the adsorption simulation starts, as shown in Fig. 1. The simulation time is 10 ns for the pressure from 5 bar to 25 bar, and 5 ns for the pressure from 30 bar to 50 bar, considering the time to reach saturation. The molecule number of methane adsorbed into the MOF-5 framework is recorded to generate the adsorption kinetics.

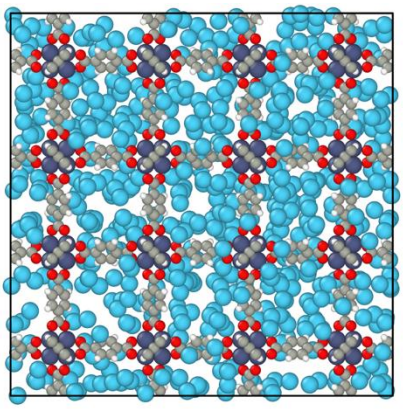

Fig. 2: The schematic of equilibrium simulation.

The equilibrium simulation is arranged to obtain the properties of adsorbed methane, such as adsorption heat and self-diffusion coefficient. It is restarted from the last sheet of the adsorption simulation, where the surrounding methane ambient are removed, exhibited as Fig. 2. Run time is 1 ns for relaxation and 200 ps for production. Energy, RDF, and MSD are recorded during the production period. Then, the MOF-5 is deleted, and the same simulation is done again for the pristine methane.

2.4 Post-processing method

Adsorption energy is the energy released by the gas or liquid adsorbate adsorbed onto the surface of the solid adsorbent. It is the evaluation of the strength of the molecular interaction. In MD it is calculated by Equation (4),

$$E_{adsorption} = E_{composite} - (E_{adsorbate} + E_{adsorbent}) \quad (4)$$

where E is the total energy, adsorbate denotes pristine methane with the same molecule number as the uptake; adsorbent denotes the pristine MOF-5. Due to the freeze of the MOF-5, only potential energy exists in the total energy of the adsorbent.

The self-diffusion coefficient can generally indicate the intensity of adsorption. Based on Einstein's Relations that the random walk of molecule is proportional to the displacement square, the self-diffusion coefficient is calculated from MSD, as shown in Equations (5) and (6),

$$MSD = \frac{1}{N}\sum_{k=1}^{N}|\vec{r}(t) - \vec{r}(0)|^2 \quad (5)$$

$$D_{self} = \lim_{t\to\infty}\frac{1}{2d}\frac{MSD}{t} \quad (6)$$

Where $\vec{r}(t)$ is the position of a molecule at time t, $\vec{r}(0)$ is the initial position, N is the number of molecules, d is the simulation dimension, and t is the simulation time. All the post-processing analysis is conducted by Python.

3. Result

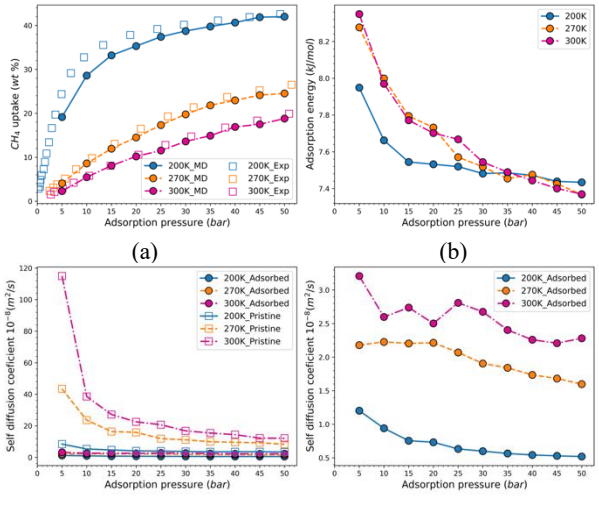

Fig. 3: Properties of adsorbed methane. (a) Adsorption isotherm. (b) Adsorption energy. (c) Self-diffusion coefficient compared to pristine methane. (d) Self-diffusion coefficient of adsorbed methane.

After the adsorption simulations, the average number of methane molecules adsorbed within the MOF-5 framework during the final 20 % of the simulation time is calculated to determine the equilibrium adsorption uptake. The equilibrium adsorption uptake under various conditions was then compiled to plot the isothermal adsorption curves shown in Fig. 3(a). These results closely agree with the uptake measured by Zhou et al.[42], where the mean relative error is less than 6 %. using the volumetric method. The unit is a percentage of the adsorbate to adsorbent mass, which is consistent with the referenced study.

Subsequently, combined with the simulation results of pristine methane, the adsorption energy and self-diffusion coefficients are calculated. Since physical adsorption is a spontaneous process, the adsorption energy is negative. For ease of representation, the absolute value of adsorption energy is used in Fig. 3(b). In this study, methane adsorption is governed entirely by van der Waals forces, with adsorption energies around 8 kJ/mol, consistent with the physical nature of the process.

As shown in Fig. 3(b), the adsorption energy decreases with increasing pressure across all temperatures. This behavior can be attributed to the prior occupation of high-energy adsorption sites, such as those near Zn atoms, by methane molecules under low-pressure conditions, resulting in higher average adsorption energies. As the pressure increases, other less favorable adsorption sites are also filled by methane, leading to a reduction in the average adsorption energy.

At high-pressure regions, the adsorption energy at 200 K approaches saturation, indicating that the distribution of adsorbed molecules has become saturated. This conclusion is supported by the isothermal adsorption curve in Fig. 3(a), where the increase in adsorption uptake at 200 K becomes nearly constant in the high-pressure region. In contrast, the adsorption uptake at 270 K and 300 K have not yet reached saturation, and thus their adsorption energy trends do not exhibit significant changes.

Additionally, in the low-pressure region, the adsorption energy at 270 K and 300 K is higher than that at 200 K. Higher temperatures result in significantly lower adsorption uptake, allowing molecules to occupy high-energy adsorption sites more readily. However, in the high-pressure region, the adsorbed phase at low temperatures tends to transition toward a liquid-like state, making it more stable than the adsorbed phase at higher temperatures. The specific nature of the adsorbed phase will be further discussed in the RDF section below.

Figure 3(c) compares the self-diffusion coefficients of adsorbed methane with those of pristine methane. According to NIST/REFPROP, pristine methane at the given densities exists in a supercritical state. With increasing pressure, the self-diffusion coefficient decreases due to the denser molecular distribution, which impedes free diffusion. Additionally, as the temperature decreases, the self-diffusion coefficient also decreases, attributed to the reduction in molecular kinetic energy at lower temperatures.

Upon adsorption, the self-diffusion coefficient of methane molecules drops significantly, by one to two orders of magnitude. This indicates that the motion of adsorbed molecules is highly restricted within the MOF-5 framework. Referring to Fig. 3(d), in addition to pressure and temperature, MD simulations also introduce computational variability.

At 300 K and 270 K, the self-diffusion coefficients are not strictly monotonic. This inconsistency arises from large oscillations in the adsorption dynamics curves at these temperatures during the simulations (shown in Fig. 4), leading to errors in the final frame adsorption uptake, which are not representative. Adjustments to the adsorption uptake are required, along with multiple independent equilibrium simulations to obtain averaged values. In contrast, the monotonicity at 200 K is significantly better due to the more stable adsorption dynamics curves at this temperature.

In Fig. 4, the diffusion is divided into two parts: interface diffusion and pore diffusion. At the beginning of adsorption, the material is nearly empty, providing a strong pressure difference at the interface between the bulk gas and adsorbent. Therefore, the uptake according to the time is close to linear. After the pore of adsorbent containing a part of adsorbate, the adsorption speed decreases, where the uptake growth is limited until approaches equilibrium. Pore diffusion dominates in this period.

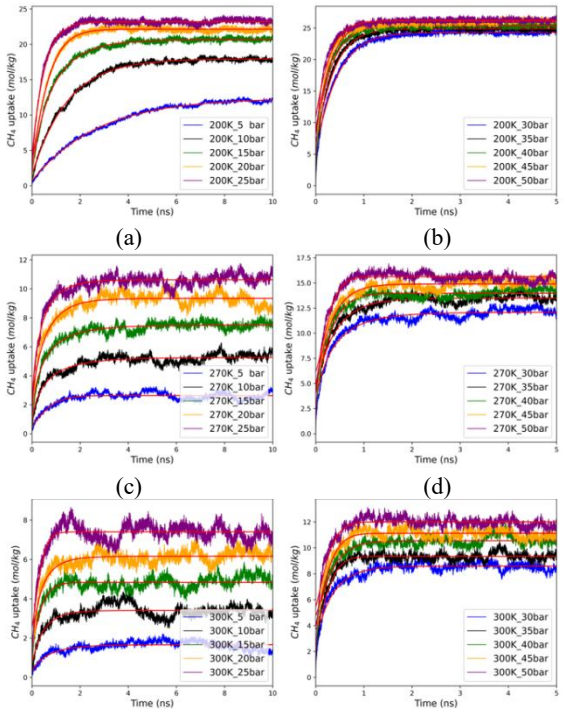

Fig. 4: Adsorption kinetics and fitting. (a) 5-25 bar at 200K, (b) 30-50 bar at 200K, (c) 5-25 bar at 270K, (d) 30-50 bar at 270K, (e) 5-25 bar at 300K, (f) 30-50 bar at 300K.

For the subsequent analysis of the adsorption kinetics, we fit those profiles first, by the medicated LDF model, which is raised by Sultan et al.[43]. The LDF model refers to Equation (7),

$$\frac{\partial w}{\partial t} = \frac{F_0 D_{surf}}{R_p^2}(w_e - w) \quad (7)$$

$$\frac{\partial w}{\partial t} = \frac{15m}{t}\theta_t^m(w_e - w) \quad (8)$$

$$\theta_t = \frac{D_{surf}}{R_p^2}t \quad (9)$$

Where F_0 is the shape factor. For spherical adsorbent particles, the value is considered as a constant of 15. D_{surf} is the surface diffusion coefficient. Rp is the adsorbent particle radium. w is adsorption uptake depends on time, and w_e is the equilibrium uptake. Sultan et al. included a dimensionless time parameter θ_t, and added a fitting factor m, as shown in Equation (8) and (9)[28]. Yang et al. used Sultan's model to investigate the R32 adsorbed in MSC30 activated carbon and found the introduction of fitting factor m gives an accurate prediction than the LDF model[44]. After integrating the Sultan's model, an integration constant C appears. Considering the physical meaning, the kinetics model is concluded as Equation (11), where w_m is the modification for uptake. Yang et al called it initial adsorption uptake, but MD has no initial adsorption, so it is treated as a modification factor.

$$w = -\exp\left[-15\left(\frac{D_{surf}}{R_p^2}t\right)^m\right]\mathrm{C} + w_e \quad (10)$$

$$w = \exp\left[-15\left(\frac{D_{surf}}{R_p^2}t\right)^m\right](w_m - w_e) + w_e \quad (11)$$

The fitted results are represented by the red curves in Fig. 5, which agree well with the simulation data, where the root mean square (RMS) is around 0.1-0.3. Particularly in the low-pressure adsorption range (Fig. 5(a), (c) and (e)). However, deviations between the fitted results and simulation data are observed during the initial stages of high-pressure adsorption (Fig. 5(b), (d) and (f)), indicating certain mathematical limitations of the model.

Additionally, we find the parameters used in the Sultan's model show strong linear trend in 200K, because of its stability of the curves. To further validate the reasonableness of those parameters, a correlation matrix was calculated with the simulated uptake, self-diffusion coefficients, and adsorption energy, as shown in Fig. 5.

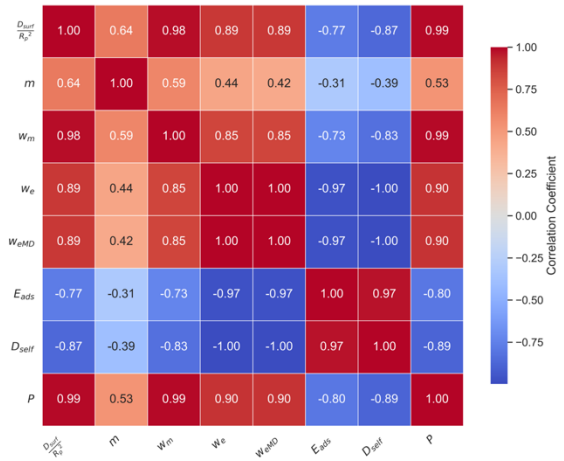

Fig. 5: Correlation metrics for parameters in Sultan's model.

Except for the fitting factor m, all other parameters exhibit strong correlations, particularly with the self-diffusion coefficient. At 200 K, the self-diffusion coefficient is completely negatively correlated with the equilibrium uptake, indicating that increasing adsorption density limits molecular diffusion. Similarly, the equilibrium uptake shows an almost perfect negative correlation with adsorption energy, further supporting the idea that increased adsorption density leads to saturation of adsorption sites.

The equilibrium uptake parameter is completely positively correlated with its simulated result w_{eMD}, which can be attributed to the boundary conditions of the kinetic model. The modification uptake factor, which also serves as a fitting variable, exhibits stronger correlations than the exponential fitting factor m, due to its linear nature.

The surface diffusion coefficient is negatively correlated with the self-diffusion coefficient. This can be understood as surface diffusion reflecting the adsorption rate, while self-diffusion represents the equilibrium adsorption configuration. At high pressures, the adsorption rate is high, but the resistance to molecular movement within the framework increases, resulting in this negative correlation.

Finally, the pressure term serves merely as a reference for correlation analysis and has no physical significance in this context.

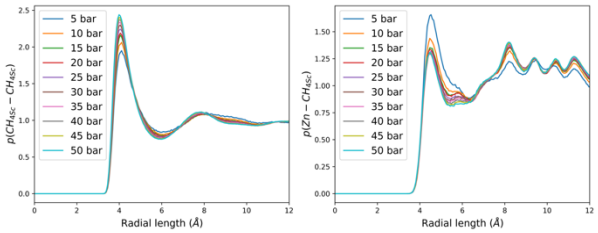

(a) (b)

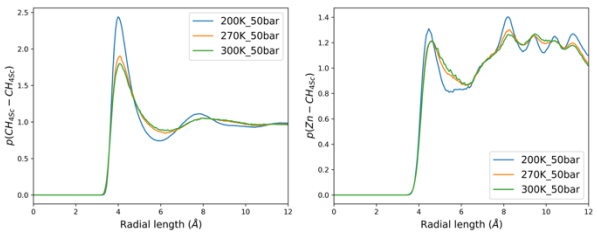

(c) (d)

Fig. 6: Radial distribution function of adsorbed methane. (a) CH4 to CH4 at 200 K. (b) Zn to CH4 at 200K. (c) CH4 to CH4 at 50 bar. (d) Zn to CH4 at 50 bar.

The state of adsorbed methane within the MOF-5 framework is discussed using RDF. Figure 6(a) presents the methane-methane RDF at 200 K, which exhibits characteristics more likely to a liquid phase. With increasing pressure, the primary peak height increases, indicating a rise in methane density. Additionally, compared to the profile at 5 bar, the secondary peak at high pressure shifts slightly to the left, suggesting a reduction in the intermolecular distance of methane molecules.

Figure 6(b) shows the Zn-methane RDF at 200 K, focusing on the comparison under low adsorption density conditions, 5 bar. As the pressure increases, the primary peak decreases while the secondary peak increases, indicating a transition in the adsorption layer's structure from monolayer adsorption to multilayer adsorption. Combined with the adsorption energy analysis, this suggests that under low pressure, methane molecules primarily occupy sites near Zn atoms. As the pressure rises, the first adsorption layer reaches saturation, and additional methane molecules begin to form subsequent adsorption layers. At other temperatures, the RDF trends with pressure are largely similar, so further detailed discussion is omitted.

For different temperatures, Fig. 6(c) reveals variations in the number of peaks in the RDF curves. At 270 K and 300 K, there are two peaks, with the second peak being very broad, indicating the beginning of a transition from a gaseous state. At 200 K, nearly three peaks are observed, with the third peak appearing only partially at the cutoff distance, suggesting that methane at 200 K approaches a liquid-like state but does not fully exhibit its characteristics. This observation agrees with the NIST assessment that all conditions correspond to the supercritical state.

In Fig. 6(d), the peaks at 200 K are noticeably narrower compared to those at 270 K and 300 K, indicating a more orderly arrangement of methane molecules, unlike the more random distribution characteristic of the gaseous state. Thus, the RDF analysis confirms that while adsorbed methane is in a supercritical state under the given conditions, the tendency toward liquid-like or gas-like behavior varies depending on the temperature and pressure.

4. Conclusion

In this study, molecular dynamics simulations were employed to investigate the adsorption behavior of methane in Cu-BTC at three temperatures, 200 K, 270 K, and 300 K, and pressures ranging from 5 bar to 50 bar. Equilibrium uptake, adsorption energy, and self-diffusion coefficients were calculated. The adsorption dynamics curves were fitted using Sultan's model, and the correlations between various parameters were analyzed. Combined with phase-state analysis using RDF, the following conclusions were drawn:

1. The LJ potential accurately captures the equilibrium adsorption behavior of methane in MOF-5, with uptake results aligning well with experimental data.
2. Methane molecules preferentially occupy high-energy adsorption sites at low pressures, resulting in higher adsorption energies. As pressure increases, methane progressively fills other adsorption sites, leading to the formation of multilayer adsorption and a subsequent decrease in adsorption energy.
3. The self-diffusion coefficient of methane decreases significantly after adsorption, indicating restricted molecular mobility. This is due both to the structural constraints of the MOF and to the transition of methane from a gaseous to a supercritical state upon adsorption, where the denser molecular arrangement reduces diffusion capacity. The relationship between adsorption energy and self-diffusion coefficient is also reflected in the correlation analysis.
4. Sultan's model generally captures the adsorption dynamics curves well but exhibits higher evaluation at the initial stages of high-pressure adsorption. Correlation analysis revealed that the surface diffusion coefficient determines the adsorption rate and is negatively correlated with the equilibrium self-diffusion coefficient.
5. Methane remains in a supercritical state after adsorption; however, depending on temperature and pressure, it may exhibit tendencies toward either a liquid-like or gas-like state. These variations also affect the distribution of adsorption layers around Zn atoms.

This study comprehensively demonstrates the methodology and application of molecular dynamics in the study of physical adsorption, providing insights that may inspire further research in this field.

Nomenclature

C	Integration constant
D	Diffusion coefficient (m^2/s)
d	Dimension (-)
F_0	Shape factor (-)
E	Energy, adsorption energy (kcal/mol) (kJ/mol)
MSD	Mean square displacement ($Å^2$) (m^2)

m	Fitting factor (-)
N	Number of molecules (-)
Rp	Adsorbent particle radius (m)
r	Distance (Å)
t	(Simulation) time (fs) (ns)
w	(Adsorption) uptake (mol/kg)

Greek symbols

θ_t	Dimensionless time factor (-)
u	Intermolecular potential (kcal/mol)
ε	Energy well depth (kcal/mol)
σ	van der Waals radius (Å)

References

1) D. Marghade, S. Shelare, C. Prakash, M.E.M. Soudagar, T.M. Yunus Khan, and M.A. Kalam, "Innovations in metal-organic frameworks (mofs): pioneering adsorption approaches for persistent organic pollutant (pop) removal," *Environmental Research*, 258 119404 (2024). doi:10.1016/j.envres.2024.119404.
2) Y. Miyah, N. El Messaoudi, M. Benjelloun, J. Georgin, D.S.P. Franco, Y. Acikbas, H.S. Kusuma, and M. Sillanpää, "MOF-derived magnetic nanocomposites as potential formulations for the efficient removal of organic pollutants from water via adsorption and advanced oxidation processes: a review," *Materials Today Sustainability*, 28 100985 (2024). doi:10.1016/j.mtsust.2024.100985.
3) F. Hussin, and M.K. Aroua, "Recent trends in the development of adsorption technologies for carbon dioxide capture: a brief literature and patent reviews (2014–2018)," *Journal of Cleaner Production*, 253 119707 (2020). doi:10.1016/j.jclepro.2019.119707.
4) X. Liu, Q. Hao, M. Fan, and B. Teng, "Carbonaceous adsorbents in wastewater treatment: from mechanism to emerging application," *Science of The Total Environment*, 955 177106 (2024). doi:10.1016/j.scitotenv.2024.177106.
5) X. Liu, S. Saren, H. Chen, J.H. Jeong, M. Li, C. Dang, T. Miyazaki, and K. Thu, "Open adsorption system for atmospheric co2 capture: scaling and sensitivity analysis," *Energy*, 294 130805 (2024). doi:10.1016/j.energy.2024.130805.
6) Y. Hou, Y. Chen, X. He, F. Wang, Q. Cai, and B. Shen, "Insights into the adsorption of co2, so2 and nox in flue gas by carbon materials: a critical review," *Chemical Engineering Journal*, 490 151424 (2024). doi:10.1016/j.cej.2024.151424.
7) A. Grich, T. Bouzid, A. Naboulsi, A. Regti, M. El Himri, and M. El Haddad, "Synthesis and optimization of activated carbon from doum (*chamaerops humilis*) fiber via pyrolysis-assisted h3po4 activation for removal of bisphenol a and α-naphthol," *Diamond and Related Materials*, 145 111061 (2024). doi:10.1016/j.diamond.2024.111061.
8) S. Ahmad, W.A. Siddiqi, and S. Ahmad, "Sustainable nanocomposite porous absorbent and membrane sieves: definition, classification, history, properties, synthesis, applications, and future prospects," *Journal of Environmental Chemical Engineering*, 11 (*2*) 109367 (2023). doi:10.1016/j.jece.2023.109367.
9) Y. Liu, Y. Qiu, Q. Zhu, and T. Tian, "Synthesis and vocs adsorption properties of diatomite/fau-type zeolite composites," *Chemical Physics Letters*, 856 141654 (2024). doi:10.1016/j.cplett.2024.141654.
10) Y. Yin, J. Wu, X. Wang, K. Ma, W. Zhai, Z. Wu, and J. Zhang, "Synthesis of zeolite molecular sieve 13x from coal-fired slag for efficient room temperature co2 adsorption," *Chemical Engineering Science*, 288 119838 (2024). doi:10.1016/j.ces.2024.119838.
11) S. Saren, S. Mitra, T. Miyazaki, K.C. Ng, and K. Thu, "A novel hybrid adsorption heat transformer – multi-effect distillation (aht-med) system for improved performance and waste heat upgrade," *Applied Energy*, 305 117744 (2022). doi:10.1016/j.apenergy.2021.117744.
12) S.V. Strelova, M.V. Solovyeva, L.G. Gordeeva, and Yu.I. Aristov, "Dynamics of water adsorption on sapo-34: comparison of three adsorbent bed configurations of adsorption chillers," *Applied Thermal Engineering*, 256 124058 (2024). doi:10.1016/j.applthermaleng.2024.124058.
13) X. Liu, S. Saren, H. Chen, M. Li, J.H. Jeong, T. Miyazaki, and K. Thu, "Dynamic performance analysis of adsorption heat transformer system driven by large pressure jump for low-grade waste heat upgrade," *Applied Energy*, 377 124478 (2025). doi:10.1016/j.apenergy.2024.124478.
14) T. Shimizu, K.K.H. De Silva, M. Hara, and M. Yoshimura, "Facile synthesis of carbon nanotubes and cellulose nanofiber incorporated graphene aerogels for selective organic dye adsorption," *Applied Surface Science*, 600 154098 (2022). doi:10.1016/j.apsusc.2022.154098.
15) N. Mushahary, A. Sarkar, F. Basumatary, S. Brahma, B. Das, and S. Basumatary, "Recent developments on graphene oxide and its composite materials: from fundamentals to applications in biodiesel synthesis, adsorption, photocatalysis, supercapacitors, sensors and antimicrobial activity," *Results in Surfaces and Interfaces*, 15 100225 (2024). doi:10.1016/j.rsurfi.2024.100225.
16) R.H. Krishna, M.N. Chandraprabha, K. Samrat, T.P. Krishna Murthy, C. Manjunatha, and S.G. Kumar, "Carbon nanotubes and graphene-based materials for adsorptive removal of metal ions – a review on surface functionalization and related adsorption mechanism," *Applied Surface Science Advances*, 16 100431 (2023). doi:10.1016/j.apsadv.2023.100431.
17) M. Wang, M. Gao, L. Deng, X. Kang, K. Zhang, Q.

Fu, Z. Xia, and D. Gao, "A sensitive and selective fluorescent sensor for 2,4,6-trinitrophenol detection based on the composite material of magnetic covalent organic frameworks, molecularly imprinted polymers and carbon dots," *Microchemical Journal*, 154 104590 (2020). doi:10.1016/j.microc.2019.104590.

18) M. Yusuf, R. Kumar, M. Ali Khan, M.J. Ahmed, M. Otero, S. Muthu Prabhu, M. Son, J.-H. Hwang, W. Hyoung Lee, and B.-H. Jeon, "Metal-organic framework-based composites for biogas and natural gas uptake: an overview of adsorption and storage mechanisms of gaseous fuels," *Chemical Engineering Journal*, 478 147302 (2023). doi:10.1016/j.cej.2023.147302.
19) M. Fakhraei Ghazvini, M. Vahedi, S. Najafi Nobar, and F. Sabouri, "Investigation of the mof adsorbents and the gas adsorptive separation mechanisms," *Journal of Environmental Chemical Engineering*, 9 (*1*) 104790 (2021). doi:10.1016/j.jece.2020.104790.
20) P. Ramirez-Vidal, G. Sdanghi, A. Celzard, and V. Fierro, "High hydrogen release by cryo-adsorption and compression on porous materials," *International Journal of Hydrogen Energy*, 47 (*14*) 8892–8915 (2022). doi:10.1016/j.ijhydene.2021.12.235.
21) Y. Ligen, H. Vrubel, and H. Girault, "Energy efficient hydrogen drying and purification for fuel cell vehicles," *International Journal of Hydrogen Energy*, 45 (*18*) 10639–10647 (2020). doi:10.1016/j.ijhydene.2020.02.035.
22) V. Kudiiarov, J. Lyu, O. Semyonov, A. Lider, S. Chaemchuen, and F. Verpoort, "Prospects of hybrid materials composed of mofs and hydride-forming metal nanoparticles for light-duty vehicle hydrogen storage," *Applied Materials Today*, 25 101208 (2021). doi:10.1016/j.apmt.2021.101208.
23) T. J, "State equation of the solid-gas interface layers," *Acta Chim. Hung.*, 69 311–328 (1971). https://cir.nii.ac.jp/crid/1572824500054794496 (Accessed date September 29, 2024)
24) D.M. M, "The equation of the characteristic curve of activated charcoal," *Dokl. Akad. Nauk. SSSR.*, 55 327–329 (1947). https://cir.nii.ac.jp/crid/1573950400604554624 (Accessed date September 29, 2024)
25) S. Brunauer, P.H. Emmett, and E. Teller, "Adsorption of gases in multimolecular layers," *J. Am. Chem. Soc.*, 60 (*2*) 309–319 (1938). doi:10.1021/ja01269a023.
26) E. Glueckauf, "Theory of chromatography. part 10.—formulæ for diffusion into spheres and their application to chromatography," *Trans. Faraday Soc.*, 51 (*0*) 1540–1551 (1955). doi:10.1039/TF9555101540.
27) A.K. Surela, L.K. Chhachhia, V.K. Surela, and P.L. Meena, "Polypyrrole-Based Composites for Dyes Removal From Contaminated Water," in: Reference Module in Materials Science and Materials Engineering, Elsevier, 2024. doi:10.1016/B978-0-323-95486-0.00019-3.
28) M. Muttakin, A. Pal, M.J. Rupa, K. Ito, and B.B. Saha, "A critical overview of adsorption kinetics for cooling and refrigeration systems," *Advances in Colloid and Interface Science*, 294 102468 (2021). doi:10.1016/j.cis.2021.102468.
29) K. Habib, B.B. Saha, K.A. Rahman, A. Chakraborty, S. Koyama, and K.C. Ng, "Experimental study on adsorption kinetics of activated carbon/r134a and activated carbon/r507a pairs," *International Journal of Refrigeration*, 33 (*4*) 706–713 (2010). doi:10.1016/j.ijrefrig.2010.01.006.
30) Q. Ke, Y. Duan, Y. Ji, D. Zhao, H. Zhang, C. Duan, L. Li, and Y. Wei, "Identical composition and distinct performance: how zif-8 polymorphs' structures affect the adsorption/separation of ethane and ethene," *J. Chem. Eng. Data*, 66 (*9*) 3483–3492 (2021). doi:10.1021/acs.jced.1c00322.
31) J. Li, Y. Li, Y. Situ, Y. Wu, W. Wang, L. Huang, C. Cai, X. Huang, Y. Guan, S. Zhang, H. Li, L. Li, Y. Zhao, H. Liang, and Z. Qiao, "Unraveling the separation mechanism of gas mixtures in mofs by combining the breakthrough curve with machine learning and high-throughput calculation," *Chemical Engineering Science*, 299 120470 (2024). doi:10.1016/j.ces.2024.120470.
32) S. Saren, H. Chen, F. Miksik, T. Miyazaki, and K. Thu, "Investigating the impact of pore structure and surface chemistry on co2 adsorption in graphitic slit-pores using gcmc simulation," *Colloids and Surfaces A: Physicochemical and Engineering Aspects*, 684 133113 (2024). doi:10.1016/j.colsurfa.2023.133113.
33) S. Siwaipram, P.A. Bopp, P. Ponchai, J.-C. Soetens, J. Hasegawa, R. Schmid, and S. Bureekaew, "MD studies of methanol confined in the metal-organic framework mof mil-88b-cl," *Journal of Molecular Liquids*, 359 119252 (2022). doi:10.1016/j.molliq.2022.119252.
34) H. Chen, S. Saren, X. Liu, J.H. Jeong, T. Miyazaki, Y.-D. Kim, and K. Thu, "Impact of adsorption on thermal conductivity dynamics of adsorbate and adsorbent: molecular dynamics study of methane and cu-btc," *IScience*, 110449 (2024). doi:10.1016/j.isci.2024.110449.
35) D. Dubbeldam, S. Calero, D.E. Ellis, and R.Q. Snurr, "RASPA: molecular simulation software for adsorption and diffusion in flexible nanoporous materials," *Molecular Simulation*, 42 (*2*) 81–101 (2016). doi:10.1080/08927022.2015.1010082.
36) C.L. Brooks, "Computer simulation of liquids," *J Solution Chem*, 18 (*1*) 99–99 (1989). doi:10.1007/BF00646086.
37) A.K. Rappe, C.J. Casewit, K.S. Colwell, W.A. Goddard, and W.M. Skiff, "UFF, a full periodic table force field for molecular mechanics and molecular dynamics simulations," *J. Am. Chem. Soc.*, 114 (*25*) 10024–10035 (1992). doi:10.1021/ja00051a040.

38) S.L. Mayo, B.D. Olafson, and W.A. Goddard, "DREIDING: a generic force field for molecular simulations," *J. Phys. Chem.*, 94 (*26*) 8897–8909 (1990). doi:10.1021/j100389a010.
39) A.P. Thompson, H.M. Aktulga, R. Berger, D.S. Bolintineanu, W.M. Brown, P.S. Crozier, P.J. in 't Veld, A. Kohlmeyer, S.G. Moore, T.D. Nguyen, R. Shan, M.J. Stevens, J. Tranchida, C. Trott, and S.J. Plimpton, "LAMMPS - a flexible simulation tool for particle-based materials modeling at the atomic, meso, and continuum scales," *Computer Physics Communications*, 271 108171 (2022). doi:10.1016/j.cpc.2021.108171.
40) D.J. Evans, and B.L. Holian, "The nose–hoover thermostat," *J. Chem. Phys.*, 83 (*8*) 4069–4074 (1985). doi:10.1063/1.449071.
41) M.L. Huber, E.W. Lemmon, I.H. Bell, and M.O. McLinden, "The nist refprop database for highly accurate properties of industrially important fluids," *Ind. Eng. Chem. Res.*, 61 (*42*) 15449–15472 (2022). doi:10.1021/acs.iecr.2c01427.
42) W. Zhou, H. Wu, M.R. Hartman, and T. Yildirim, "Hydrogen and methane adsorption in metal−organic frameworks: a high-pressure volumetric study," *J. Phys. Chem. C*, 111 (*44*) 16131–16137 (2007). doi:10.1021/jp074889i.
43) M. Sultan, I.I. El-Sharkawy, T. Miyazaki, B.B. Saha, S. Koyama, T. Maruyama, S. Maeda, and T. Nakamura, "Water vapor sorption kinetics of polymer based sorbents: theory and experiments," *Applied Thermal Engineering*, 106 192–202 (2016). doi:10.1016/j.applthermaleng.2016.05.192.
44) Z. Yang, M. Sultan, K. Thu, and T. Miyazaki, "Experimental investigation and thermodynamic modeling of adsorption equilibria of msc30 with r32 for supercritical adsorption cooling systems," *International Journal of Heat and Mass Transfer*, 219 124873 (2024). doi:10.1016/j.ijheatmasstransfer.2023.124873.